Evolutionarily conserved transcriptional regulators control monoaminergic neuron development

Clifton Lewis[1,2,11], Matthew Goulty[1,3], Aniela Wroblewska[1], Nicola Croxall[4], David Onion[4], Sue Robinson[5], Robert P. Zinzen[6], Jordi Solana[7,8], Charlambos P. Kyriacou[1], Ezio Rosato[1], Roberto Feuda[1,9,10]

[1] Neurogenetics Group, Division of Genetics and Genome Biology, School of Biology and Biomedical Sciences, College of Life Sciences, University of Leicester, Leicester LE1 7RH, UK

[2] Centre for Chromosome Biology, Biomedical Sciences Building, University of Galway, Galway, H91 W2TY, Ireland

[3] The Francis Crick Institute, London, UK

[4] Faculty of Medicine & Health Sciences, Queen's Medical Centre, Nottingham NG7 2UH, UK

[5] Division of Molecular and Cell Biology, College of Life Sciences, University of Leicester, Leicester LE1 7RH, UK

[6] Systems Biology Imaging Technology Platform, Max Delbrück Centre for Molecular Medicine (MDC-BIMSB), Berlin, Germany

[7] Living Systems Institute, University of Exeter, Exeter, UK

[8] Department of Biosciences, University of Exeter, Exeter, UK

[9] Department of Biology, Geology and Environmental Science, University of Bologna, Bologna, Italy

[10] Correspondence: rf190@leicester.ac.uk / roberto.feuda@unibo.it (R.F.)
[11] Correspondence: clifton.lewis@leicester.ac.uk / clifton.lewis@universityofgalway.ie (C.L.)

Abstract

To what extent conserved developmental programs specify homologous cell types is a central question in biology. Here, we address this by focusing on reconstructing monoaminergic neuron development in *Drosophila melanogaster* embryo using time-resolved single-cell genomics, spatial transcript mapping with hybridisation chain reaction, and targeted metabolomics. We uncover a regulatory landscape in which specific transcription factors are activated before biosynthetic enzymes, establishing a prospective temporal architecture for monoaminergic fate specification. Comparative analyses of developmental single-cell atlases from zebrafish and sea urchin indicate that components of this machinery are conserved across ~550 million years of bilaterian evolution with orthologous transcription factors showing similar temporal dynamics. Together, these findings point to a putatively conserved regulatory core that interfaces with other context-dependent transcription factors; this interplay accommodates monoaminergic multifunction and subtype diversity across distinct neuroanatomies.

Introduction

Understanding whether conserved or divergent developmental programs underlie the specification of homologous cell types is a central goal in evolutionary and developmental biology. We address this question by focusing on monoaminergic neurons, a class of cells that produce neuromodulators such as dopamine and serotonin. Monoaminergic neurons provide a powerful system to study evolution and development for several reasons. They are molecularly defined by the expression of key biosynthetic enzymes (Libersat and Pflueger, 2004), they are widespread across bilaterians, their monoamine products can be precisely quantified, and the genes underlying their biosynthetic pathways have been shown to derive from a common evolutionary origin (Parent, 1984; Yamamoto and Vernier, 2011; Goulty *et al.*, 2023).

Although these neurons are extremely rare (<1% of neurons in fly and mammalian brains), they play fundamental roles in processes ranging from motor control and circadian rhythms to learning and mood (Libersat and Pflueger, 2004; Flames and Hobert, 2011; Monti, 2011; Waddell, 2013; Zheng *et al.*, 2025). Furthermore, their dysfunction contributes to major human neurological and psychiatric disorders, including Parkinson's disease, depression, and schizophrenia (Kurian *et al.*, 2011; Volkow *et al.*, 2011; Grace, 2016).

The developmental specification of monoaminergic neurons requires the coordinated activity of multiple transcription factors (TFs) and other regulatory genes organised into hierarchical gene regulatory networks (GRNs) (Hobert, 2008; Flames and Hobert, 2009, 2011). Studies across vertebrates and invertebrates have identified TFs that are critical for establishing monoaminergic fate (Flames and Hobert, 2011). In vertebrates, for example, LIM-homeodomain proteins Lmx1a/b, the ETS factor Fev/Pet-1, and Nkx2.2 are essential for serotonergic neuron specification (Cheng *et al.*, 2003; Ding *et al.*, 2003; Hendricks *et al.*, 2003). In *Drosophila*, the zinc-finger proteins Eagle (eg) and Huckebein (hkb) play similar roles in serotonergic differentiation (Dittrich *et al.*, 1997). In *C. elegans*, dopaminergic fate is controlled by terminal selector TFs such as the ETS transcription factor, AST-1 (Flames and Hobert, 2009). Previous work from our lab established that monoaminergic cell identity is defined by a conserved set of transcription factors shared across bilaterian species, suggesting that a common regulatory basis for these neurons originated early in animal evolution (Goulty *et al.*, 2025). Yet these candidate-based studies provide only

a partial view of the regulatory landscape underlying monoaminergic specification and their possible conservation. We therefore still lack a systems-level understanding of how monoaminergic neurons develop. Addressing these questions is essential for understanding whether homologous cell-types develop following a conserved transcriptional program.

Here to address this open question, we combine time-resolved single-cell transcriptomics, trajectory modelling, spatial transcript validation, and targeted metabolomics in embryonic neurogenesis of *Drosophila melanogaster*, and test for evolutionary conservation in zebrafish and sea urchin development. Our results reveal the developmental program of monoaminergic neurons in the *Drosophila* embryo, including key TFs—*fd59A*, *dmrt99B*, and *Lmx1a*—that pattern these lineages and differences in maturation rates between subtypes. We also identified several TF orthogroups conserved across *Drosophila*, sea urchin, and zebrafish. Comparison of monoaminergic developmental trajectory between *Drosophila* and zebrafish revealed a similar developmental cascade of TFs. Together, these findings support a putative conserved temporal logic for monoaminergic fate acquisition and begin to explain how developmental fate and function can align and/or diverge across species.

Results

A temporally resolved single-cell atlas captures neurogenesis in *Drosophila*. To understand the development of monoaminergic neurons, we performed single-cell RNA sequencing (scRNA-seq) on *Drosophila melanogaster* embryos collected at eight partially overlapping time windows spanning 0 to 22 hours after egg laying (AEL), with two biological replicates per window (**Figure 1A.**), covering the transition from neuroectoderm to fully differentiated embryonic neurons. To enrich for progenitor and early neural population, we used a SoxN-sfGFP transgenic line (VDRC #318062, Sarov *et al.*, 2016) to isolate proneural cells and neuroblasts, and anti-Elav immunostaining to enrich for differentiating neurons, followed by fluorescence-activated cell sorting (FACS) (**Figure S1.**). Single cell RNA-seq libraries were prepared on the 10X Genomics v3.1 platform and sequenced using Illumina NovaSeq X Plus.

After standard quality control, we retained 57,476 high-quality cells, resolving into transcriptionally distinct clusters. Cluster identities were assigned by mapping

108 cluster-specific marker genes—selected as the top differentially expressed features
109 with adjusted p-value < 0.05—to *in situ* expression patterns from the Berkeley
110 Drosophila Genome Project (BDGP) using an annotation pipeline adapted from
111 Calderon *et al.* (2022). This analysis revealed a clear temporal transition: early clusters
112 were enriched for maternal and early zygotic genes, whereas later stages featured
113 organised, differentiated tissues; including the brain primordium, embryonic brain, and
114 embryonic gut (**Figure 1B.** and **Table S1.**). Embedding all time points together
115 revealed a continuous developmental trajectory (**Figure 1C.**), capturing the
116 progressive emergence of neuronal identity.
117
118 **Neurotransmitter subtype emergence reveals early co-expression and lineage**
119 **complexity.** Although our dataset is enriched for neural progenitors and differentiated
120 neurons, cluster annotations revealed the presence of additional cell types (**Figure**
121 **1C.**). This likely reflects autofluorescence and/or putatively *SoxN*-driven GFP
122 expression in the developing gut, leading to non-specific capture during FACS
123 enrichment (**Figure S1.**).
124 To resolve distinct stages of neurogenesis, we used established markers - e.g.
125 *dpn*, *wor*, *mir*, *elav*, *nSyb* - to identify neuroblasts, ganglion mother cells (GMCs),
126 intermediate neural progenitors (INPs), and mature neurons in a population of ~40,000
127 cells (**Figure 2A.**, **Figure S3A.**) (Dillon *et al.*, 2022; Peng *et al.*, 2024). To capture the
128 full neurogenic continuum, spanning from neuroblasts to mature neurons, we
129 subsampled to ~10,000 high-quality cells, excluding disparate clusters (**Figure 2B.**,
130 **Figure S3B.**). These cells were distributed across all the developmental time points,
131 enabling the reconstruction of continuous differentiation trajectories (**Figure 2C.**).
132 Among these terminal-state mature neurons, we identified seven neurotransmitter-
133 defined populations: cholinergic (931 cells), GABAergic (816 cells), glutamatergic (173
134 cells), monoaminergic (77 cells), and three mixed populations co-expressing markers
135 of GABA and glutamate (100 cells), acetylcholine and GABA (556 cells), or serotonin
136 and GABA (388 cells), respectively (**Figure 2B.**).
137 Given that distinct TF combinations are known to contribute to neuronal subtype
138 identity, we next sought to identify TFs associated with each neurotransmitter-defined
139 population (**Figure 2E.**). Our differential TF expression analysis revealed that, with the
140 exception of neuroblasts/GMCs, GABA/glutamatergic neurons, and monoaminergic
141 neurons, most of these neuronal populations could not be unambiguously resolved

142 based on TF expression alone. This outcome suggests that TFs in these other
143 lineages may lack strict subtype specificity, that neuronal identity may arise from more
144 complex regulatory interactions beyond TF expression, or that the dataset may not
145 have sufficient depth to fully resolve these distinctions. Monoaminergic neurons,
146 however, showed co-expression of multiple TFs, including *fd59A*, *dmrt99B*, *Lmx1a*,
147 and *Vsx1* and *Vsx2* (**Figure 2E.**). In contrast, the mixed serotonergic/GABAergic
148 population was marked by the co-expression of *CG8301* and *br* (**Figure 2E.**). These
149 findings define candidate regulatory genes underlying monoaminergic fate.
150
151 **RNA velocity reveals continuous differentiation trajectories.** To investigate the
152 transcriptional dynamics underlying monoaminergic neuron differentiation, we applied
153 RNA velocity analysis using scVelo (La Manno *et al.*, 2018; Bergen *et al.*, 2020) and
154 modelled lineage trajectories with CellRank (v2) (Lange *et al.*, 2022; Weiler *et al.*,
155 2024), which integrates splicing kinetics (Velocity Kernel), transcriptomic similarity
156 (Connectivity Kernel), and CytoTRACE dynamics to infer directed developmental
157 transitions (CytoTRACE Kernel). We first applied scVelo to the full dataset. Velocity
158 vector fields projected onto the UMAP embedding revealed a strong correlation
159 between transcriptional dynamics and the temporal structure of the dataset (**Figure**
160 **S4**).

161 We then focused on the subclustered population spanning the full neurogenic
162 trajectory from neuroblasts to mature neurons (**Figure 2B–D**). Application of scVelo
163 and CellRank to this dataset recovered clear trajectories for each subtype and a
164 smooth latent-time ordering (**Figure S5A**). To interpret the underlying programs, we
165 identified velocity-inferred dynamical genes with the scVelo dynamical model and
166 ordered cells by latent time (**Figure S5B.**). We discretised latent time into 20 bins and,
167 for each bin, compiled the genes whose fitted expression/velocity profiles peaked
168 within that interval. Gene Ontology (GO) over-representation analyses (ORA) were
169 then performed using all expressed genes in the subset as background with
170 Benjamini–Hochberg correction. The enrichment landscape shows a coherent
171 progression: (i) early bins are dominated by cell-state remodelling and tissue-building
172 programs—RNA processing, cell cycle/proliferation, morphogenesis, and
173 organogenesis; (ii) intermediate bins transition toward neuronal differentiation, with
174 terms related to synapse formation and cell morphogenesis involved in neuron

175 differentiation; while (iii) late bins are enriched for synaptic and excitability modules,
176 including neuron recognition, axon guidance, and neuroactive ligand–receptor
177 interaction, consistent with the acquisition of functional neuronal properties. Together,
178 these GO trends align with the velocity-derived latent-time ordering and provide
179 functional support for a continuous maturation from progenitor states to functionally
180 specialised neurons (**Figure S5C.**).

181 To reconstruct the differentiation trajectory of monoaminergic neurons in
182 greater detail, we applied CellRank to define initial and terminal states and to model
183 transcriptional dynamics within this specific lineage (**Figure 3A**). Genes encoding key
184 enzymes required for monoaminergic neurotransmission—including *ple*, *Tdc1*, *Tdc2*,
185 *Tbh*, and *Vmat*—were strongly upregulated toward the terminal state, as expected,
186 marking the final stages of differentiation. With the exception of *Trhn* and *Ddc*, these
187 enzymes exhibited high specificity for the monoaminergic lineage (**Figure S6.**),
188 indicating subtype-restricted induction of the biosynthetic program. Similarly, top-
189 ranking TFs associated with monoaminergic identity—including *fd59A*, *dmrt99B*, and
190 *Lmx1a*—were also selectively expressed in the monoaminergic trajectory (**Figure 3B.**)
191 and peaked at approximately the same latent time as the biosynthetic genes (**Figure**
192 **3A.**). This coordinated expression suggests a tightly coupled regulatory program in
193 which TFs may directly activate terminal differentiation effectors. In contrast—and
194 consistent with their role as responders to monoamine signals—genes encoding
195 monoaminergic receptors showed broader expression across multiple neuronal
196 lineages (**Figure S7.**). This pattern suggests that receptor deployment is decoupled
197 from biosynthetic identity and instead reflects widespread postsynaptic
198 responsiveness to monoamines.
199

200 **Spatial validation supports coordinated transcriptional activation and resolves**
201 **monoaminergic subtype identity.** Although our scRNA-seq atlas resolves the major
202 neuronal lineages and transmitter classes, monoaminergic neurons are a rare
203 population in the *Drosophila* CNS (Busch *et al.*, 2009; Hartenstein *et al.*, 2017; Kasture
204 *et al.*, 2018; Babski, Codianni and Bhandawat, 2024). As a result, it was difficult to
205 clearly separate specific monoaminergic subtypes from transcriptomes alone. To both
206 validate CellRank-inferred dynamics and add spatial specificity, we focused on two

207 subtypes – serotonergic and dopaminergic - and performed hybridisation chain
208 reaction (HCR) (Choi *et al.*, 2018)**.**

209 We assayed a panel that included most of the monoaminergic biosynthetic
210 enzymes, their receptors, and six transcription factors (**Figure 4.**, **Figure S8-9.**). TFs
211 were chosen based on differential expression within the monoaminergic lineage
212 (**Figure 2C.**) and prior evidence for roles in monoaminergic fate. Spatial profiling
213 showed that *fd59A*, *dmrt99B*, and *Lmx1a* are expressed in the CNS beginning at
214 stages 10–12 (~8 h AEL), preceding the onset of biosynthetic gene expression. In
215 contrast, monoaminergic enzymes were robustly expressed from stage 12 (~10 h
216 AEL) onward, consistent with the timing of neuronal specification. Notably, this TF
217 induction occurs slightly earlier than suggested by our latent-time analysis, which
218 predicted a more coordinated co-activation with the enzymes. Receptors generally
219 followed a similar onset, with most appearing from stage 12. A notable exception was
220 *5-HT2A*, which was detected as early as stage 1 and in non-neural tissues, consistent
221 with a recent study implicating it in early morphogenetic roles beyond
222 neurotransmission (Karki *et al.*, 2023)**.**

223 Together, these data mostly corroborate the temporal ordering inferred by
224 CellRank and, crucially, resolve subtype identity by localising expression to
225 serotonergic or dopaminergic domains. They further suggest that these TFs, *fd59A*,
226 *dmrt99B*, and *Lmx1a*, may act upstream to specifically initiate part of the
227 monoaminergic program, with effector enzymes and receptors switching on
228 subsequently.

229

230 **Mass spectrometry reveals temporally distinct onset of monoamine production.**
231 Our transcriptional and spatial analyses suggests that by stage 12 (~9–10 h AEL), the
232 *Drosophila* embryo expresses the biosynthetic enzymes and receptors required to
233 produce and respond to monoamines. However, whether these neurons are
234 functionally active at this stage remains unresolved. Previous studies have detected
235 serotonin and dopamine via immunohistochemistry only from stage 17 (~15 h AEL)
236 onwards (Lundell and Hirsh, 1994), raising questions about the relationship between
237 transcriptional commitment and neurotransmitter availability. To resolve this
238 dichotomy, we conducted targeted mass spectrometry across seven developmental
239 windows spanning 0–22 h AEL. At each time point, we analysed ≥6 biological

240 replicates (54 samples total) and quantified 19 analytes, including all canonical
241 monoamines (**Table S2.**) GABA, glutamate, and acetylcholine **(Figure S11.).**
242 Our results revealed distinct temporal profiles across monoaminergic subtypes
243 (**Figure 5.; Figure S10.**). Histamine and tyramine were constitutively present
244 throughout development, suggesting their production may occur independently of
245 canonical neurogenesis. In contrast, both dopamine and serotonin exhibited
246 temporally restricted accumulation, with sharp increases after stage 12—closely
247 aligning with the transcriptional induction of their biosynthetic enzymes. Although
248 dopamine and serotonin followed similar temporal trajectories, their relative levels
249 differed, likely reflecting variations in biosynthetic efficiency or substrate availability. It
250 is important to note that this effect may also reflect differences in the detection
251 capabilities for these molecules.
252 Together, these findings indicate that transcriptional programs broadly predict
253 the functional potential of monoaminergic neurons, but the timing and extent of
254 neurotransmitter production are modulated by subtype-specific biochemical properties
255 and/or regulatory constraints.
256
257 **Conserved transcriptional dynamics underpin monoaminergic neuron**
258 **development in *Drosophila* and zebrafish.** Monoaminergic neurons are widely
259 distributed across bilaterian animals, yet whether they arise from a conserved
260 developmental program remains unclear. Our findings in *Drosophila* suggest that a
261 specific set of TFs are activated during monoaminergic neuron differentiation,
262 providing an opportunity to test the evolutionary conservation of this regulatory
263 program. To address this question, we reanalysed published developmental single-
264 cell RNA-seq data from *Danio rerio* and sea urchin, *Strongylocentrotus purpuratus*.
265 For *Danio rerio*, we reprocessed a developmental time series spanning embryonic to
266 larval stages (10 hours post-fertilisation [hpf] 232 to 10 days post-fertilisation [dpf];
267 Lange *et al.*, 2024). For *S. purpuratus*, we merged two complementary datasets,
268 covering the 8-cell embryo through the 72 hpf larval stages (Foster, Oulhen and
269 Wessel, 2020; Perillo *et al.*, 2020). Central nervous system cell types were annotated
270 using orthologous marker genes applied previously in *Drosophila* (**Figure 2D.**) and
271 identified monoaminergic neuron populations based on expression of canonical
272 biosynthetic genes (**Figure S12A-B.**).

273 Applying the same differential-expression (DE) criteria used in fly (adjusted $p <$
274 0.05; $|\log_2 FC| \geq 0.25$), we identified transcription factors (TFs) enriched in zebrafish
275 and sea urchin monoaminergic clusters analysed independently (**Figure 6A.**; **Table**
276 **S3**). We analysed clusters separately, rather than collapsing them into a single
277 monoaminergic group, to gather an inclusive list of TFs that define monoaminergic
278 identity across subtypes. To enable cross-species comparisons despite lineage-
279 specific duplications, genes were mapped to bilaterian-level eggNOG orthogroups.
280 Orthologs of key fly regulators were recovered in vertebrates, including *lmx1a* paralogs
281 (*lmx1a*, *lmx1al*, *lmx1ba*). In total, 15 TF orthogroups were differentially expressed in
282 both fly and zebrafish monoaminergic neurons, and 16 TF orthogroups were shared
283 between fly and sea urchin (**Figure 6C.**; **Table S4.**), defining a set of putative
284 conserved regulators. Notably, six TF orthogroups—*CG8301*, *Lmx1a*/*CG4328*, *Hr3*,
285 *Eip78C*, *net*, and *Pdp1*—were shared across all three species comparisons,
286 underscoring a potentially conserved core program for monoaminergic identity. The
287 partial overlap of the remaining TFs suggests that, while a conserved regulatory core
288 might exist, additional factors have diverged or been co-opted in lineage-specific
289 contexts
290 To test whether this conservation was unique to monoaminergic neurons, we
291 repeated the orthogroup-level analysis between *Drosophila* and zebrafish for other
292 neurotransmitter classes (Acetylcholine, GABA, Glutamate; **Figure S13.**). The number
293 of shared DE TF orthogroups was of similar magnitude across classes, despite vastly
294 different neuronal population sizes, supporting a model in which each transmitter
295 lineage may share a small, conserved set of regulators that is then diversified by
296 lineage- and species-specific additions.
297 We next asked whether not only TF identity but also their temporal activation is
298 conserved. Using the comparable time-resolved zebrafish dataset, we applied RNA
299 velocity and CellRank to reconstruct differentiation dynamics. Several orthologous
300 TFs, including *lmx1* paralogs, showed late upregulation along the zebrafish
301 monoaminergic trajectory, closely mirroring the dynamics observed in *Drosophila*
302 (**Figure 6B.**). Thus, some of the regulatory content and timing of activation are aligned
303 between insects and vertebrates, at least in these representative species.
304 Together, these findings support a model in which monoaminergic neurons
305 emerge from a potential conserved transcriptional program, with shared regulators,
306 such as *Lmx1a*, but critically has undergone significant species-specific elaborations.

Discussion

The extent to which homologous cell types are specified by conserved developmental and transcriptional programs remains a central question in evolutionary developmental biology. Monoaminergic neurons, which play fundamental roles in neurotransmission across bilaterians, offer a powerful model for addressing this issue. Previous comparative transcriptomic analyses have suggested that monoaminergic cell identity is defined by a shared set of transcription factors, indicating an origin in the bilaterian stem lineage (Goulty *et al.*, 2025). Yet, whether the developmental processes that give rise to these neurons are likewise conserved—or instead represent cases of convergent evolution—has remained unresolved. Additionally, by determining whether the developmental program underlying these neurons is shared across species, we further clarify the hypothesis of a conserved evolutionary origin. In this study, we characterise the transcriptional program governing monoaminergic neuron development in *Drosophila* embryos and reveal that key regulatory components are shared with vertebrate and deuterostome systems. Our findings suggest that monoaminergic neurons are specified by an evolutionarily conserved developmental framework that emerged early in bilaterian evolution.

Within *Drosophila*, we identify a regulatory program involving *fd59A*, *dmrt99B*, *Vsx1*, *Vsx2*, and *Lmx1a*. These TFs are selectively expressed in the monoaminergic lineage and become active around stage 12, coincident with the onset of biosynthetic enzyme expression (*ple*, *Tdc2*, *Tbh*, *Vmat*). Spatial validation by HCR confirmed the sequential activation of these genes and showed that TF induction precedes biosynthetic gene expression, supporting their role as primary regulators of monoaminergic fate. This organisation mirrors vertebrate serotonergic development, where Lmx1a/b and Pet-1/Fev initiate comparable programs (Ding *et al.*, 2003; Hendricks *et al.*, 2003; Flames and Hobert, 2011), pointing to deep evolutionary parallels.

Although biosynthetic gene expression initiates around stage 12, metabolomic profiling reveals pronounced differences in monoamine accumulation. Dopamine and serotonin both increase after stage 12, yet dopamine accumulates more rapidly—likely reflecting the higher catalytic efficiency of Dopa decarboxylase (Ddc) for L-3,4-dihydroxyphenylalanine (L-DOPA) than for 5-hydroxytryptophan (5-HTP), the respective intermediates in the dopamine and serotonin biosynthetic pathways

340 (Montioli and Borri Voltattorni, 2021). In contrast, octopamine remains undetectable
341 despite enzyme expression, suggesting either technical limitations or additional
342 biological constraints such as substrate availability, enzymatic kinetics, or post-
343 transcriptional control. These findings indicate that transcriptional activation alone is
344 insufficient for transmitter synthesis, pointing to additional regulatory layers that
345 modulate monoamine output. However, these interpretations remain constrained by
346 the detection sensitivity and chemical properties of the specific metabolites analysed.

347 Our comparative analysis of monoaminergic neuron development in
348 *Drosophila*, zebrafish, and sea urchins reveals a deeply conserved transcriptional
349 program, underscoring a shared regulatory logic that likely emerged early in bilaterian
350 evolution. The identification of six conserved TF orthogroups—*CG8301*,
351 *Lmx1a*/*CG4328*, *Hr3*, *Eip78C*, *net*, and *Pdp1*—establishes a core genetic program for
352 specifying monoaminergic identity. This finding supports the hypothesis that these
353 neurons represent potentially homologous cell types that originated early in bilaterian
354 evolution. Core regulatory modules specifying neuronal identity appear to have been
355 established in the bilaterian ancestor and maintained across deep evolutionary time
356 (Arendt, 2005; Arendt *et al.*, 2019; Rapti, 2022; Sachkova, Modepalli and Kittelmann,
357 2025). For instance, Lmx1a has a well-documented and critical role in the
358 development of dopaminergic neurons in vertebrates, where it regulates key effector
359 genes such as tyrosine hydroxylase (*Th*) and the dopamine transporter (*DAT*) to
360 ensure proper differentiation and maturation (Cai *et al.*, 2009; Doucet-Beaupré, Ang
361 and Lévesque, 2015). This role has not previously been demonstrated in non-
362 vertebrates, suggesting that *Lmx1a* may represent an ancient regulator of
363 monoaminergic fate specification—although convergent evolution of similar
364 transcriptional strategies cannot be excluded.

365 Importantly, this conservation is not absolute. We also observed substantial
366 regulatory divergence, with several TFs associated with monoaminergic differentiation
367 being unique to specific lineages. This pattern may reflect a dual-layered evolutionary
368 process—an ancient, conserved core program governing fate commitment,
369 complemented by lineage-specific regulators that refine neuronal subtype identity
370 (Hobert, 2008; Arendt *et al.*, 2019). Alternatively, the conserved TF set itself may
371 specify distinct monoaminergic identities across species, while divergent TFs act as
372 complementary components that integrate these core programs into broader gene-
373 regulatory networks, coordinating cross-talk and aligning specification with species-

374 specific neural architectures (Flames and Hobert, 2011; Rapti, 2022). While some
375 apparent differences may arise from technical factors (e.g., sequencing depth,
376 detection sensitivity, or annotation), others likely represent genuine regulatory
377 divergence. Given the substantial variation in neuroanatomical organisation among
378 insects, vertebrates, and echinoderms, such divergence may reflect adaptive
379 remodelling of the regulatory landscape to distinct neural architectures.

380 The temporal dynamics of conserved TFs suggest that these genes govern
381 monoaminergic fate commitment, whereas lineage-specific TFs modulate neuronal
382 subtype identity in a species-dependent manner. The hierarchical relationships
383 between conserved and lineage-specific TFs remain to be elucidated. Determining
384 whether these factors operate through feedforward or feedback regulatory loops—a
385 recurrent feature of GRN architecture that stabilises neuronal identity—will be crucial
386 (Flames and Hobert, 2011; Peter and Davidson, 2011). Understanding how conserved
387 GRNs are modified to generate lineage-specific phenotypes will be essential for
388 uncovering the general principles that govern cell-type diversification across evolution.

389 Our mass-spectrometry data indicate a partial decoupling between monoamine
390 abundance and biosynthetic enzyme expression. While enzyme kinetics may account
391 for some of the observed differences in transmitter accumulation, it remains unclear
392 whether such decoupling is a general feature of monoaminergic neurons across taxa.
393 Moreover, the functions of early monoamine signalling—potentially enabled by
394 precocious receptor expression (e.g., 5-HT2A)—during embryogenesis remain
395 unresolved.

396 Integrating transcriptomic, metabolomic, and spatial data across additional
397 bilaterian taxa will be important for testing the universality of these patterns.
398 Comparative perturbation experiments—targeting conserved TFs such as Lmx1a or
399 Hr3 in non-model systems—could determine whether shared transcriptional logic
400 indeed translates into conserved functional outcomes.

401 In conclusion, our study uncovers a conserved temporal program for
402 monoaminergic neuron specification, in which early transcription factor activation
403 orchestrates biosynthetic gene expression to align fate determination with functional
404 maturation. By linking transcriptional programs, transmitter synthesis, and receptor
405 deployment across species, our work provides a framework for understanding how
406 conserved and divergent GRNs generate neuromodulatory diversity and how neuronal
407 fate and function are developmentally coupled.

408 ## Methods

409 ### Fly husbandry

410 All *Drosophila melanogaster* stocks were maintained on standard cornmeal–yeast–
411 agar medium at 18°C or 25°C, with relative humidity held at approximately 40%. We
412 employed a transgenic SoxN–sfGFP line (VDRC #318062), which was reared
413 continuously at 25°C (Sarov *et al.*, 2016).
414

415 ### Embryo collection

416 Adult flies were transferred into population cages fitted with agar plates prepared from
417 mango juices, each supplemented with fresh yeast paste to boost fecundity. To
418 eliminate circadian-driven fluctuations in gene expression, cages were kept in constant
419 darkness (DD) beginning immediately upon transfer (Wijnen *et al.*, 2006). Following a
420 48-hour acclimation under DD, embryo collections was commenced, ensuring that all
421 developmental stages progressed without light-induced transcriptional variability.
422 Embryos were collected over eight successive, overlapping time windows
423 covering the full span of embryonic development; between 0-22 hours after egg laying
424 (AEL). Collections were performed in biological duplicate to increase data reliability
425 and resolution of transitional stages. Agar plates were replaced regularly to maintain
426 optimal oviposition conditions, and collected embryos remained in the same DD
427 incubator for precise aging.
428 Given the necessity of preserving RNA integrity for 10X Genomics single-cell
429 RNA-sequencing, we avoided formaldehyde-based fixatives. Instead, we applied
430 dithio-bis(succinimidyl propionate) (DSP; Sigma-Aldrich), a reversible cross-linker
431 compatible with downstream library preparation. A 50 mg/mL DSP stock was made in
432 DMSO, then diluted by adding 5 mL Dulbecco's PBS (DPBS; Gibco) to the 100 µL
433 stock, followed by sterilisation through a 0.2 µm syringe filter. Collected embryos were
434 fixed in this working solution, preserving stage-specific transcriptomes and enabling
435 reliable reversal of cross-links prior to sequencing.
436

437 ### Embryo Harvesting, Dechorionation, and Fixation

438 Collected embryos were gently dislodged from agar plates by rinsing with distilled
439 water and transferred into a 30 µm nylon mesh sieve using a fine paintbrush. Any
440 residual yeast paste was washed away under a gentle stream of distilled water to

441 minimise contamination. Dechorionation was performed by submerging the embryos
442 in 50% bleach (Arco Essentials) for 3 minutes, then immediately rinsing them
443 thoroughly with distilled water until all bleach was removed.
444 For fixation, equal volumes of the DSP working solution and heptane (Fisher
445 Scientific) were combined in a glass scintillation vial. Dechorionated embryos were
446 added to this biphasic mixture and incubated on a gyroscopic rocker at room
447 temperature for 1 hour, ensuring gentle but continuous agitation. After fixation, the
448 lower aqueous phase was discarded, and cold methanol (VWR) was added to the
449 heptane layer to initiate devitellinisation. Embryos were vortexed for 2 minutes to
450 facilitate complete removal of the vitelline membrane, then allowed to settle to the
451 bottom of the vial. Finally, embryos were transferred to 1.5 mL Eppendorf tubes and
452 washed three times in fresh methanol. Fixed embryos were stored at –20°C until
453 further processing.
454
455 **Immunofluorescence**
456 All immunostaining was performed at 4°C under stringent RNase-free conditions:
457 Protector RNase Inhibitor (Roche, RNAINH-RO) was added to all buffers at 5 U/mL
458 during brief washes and 20 U/mL for all longer incubations, and both bovine serum
459 albumin (BSA; Gibco) and normal goat serum (NGS; Vector Laboratories) were heat-
460 inactivated at 60°C for 30 minutes to eliminate residual RNases. Prior to antibody
461 staining, DSP–methanol–fixed embryos were gradually rehydrated through an ethanol
462 series into PBT (PBS + 0.1% Triton X-100; Sigma-Aldrich T8787) and then washed
463 three times for 10 minutes each in PBT containing RNase inhibitor, with gentle rocking
464 to ensure complete removal of the methanol fixative. To block non-specific binding,
465 embryos were incubated overnight at 4°C in PBT supplemented with 1% heat-
466 inactivated BSA and 2% heat-inactivated NGS. The embryos were then transferred
467 into fresh blocking buffer (PBT + inhibitor, 1% BSA, 2% NGS) containing primary
468 antibodies: rabbit α-GFP (1:100; Invitrogen) to label SoxN–sfGFP^{+} neurogenic cells,
469 and rat α-Elav (1:100; DSHB) to detect post-mitotic neurons. After overnight incubation
470 at 4°C with gentle agitation, excess primary antibody was removed by three 10-minute
471 washes in PBT. Secondary detection was performed by incubating embryos overnight
472 in the same blocking buffer supplemented with goat α-rabbit Alexa Fluor 488 (1:500;
473 Invitrogen), mouse α-rat PE (1:500; Invitrogen), and the nuclear counterstain DRAQ5

474 (4 µL/mL; Thermo Scientific). Finally, stained embryos were washed three times in
475 PBT (10 minutes each) and stored at 4 °C in PBT until mounting and imaging.
476
477 **Microscopy validation and processing**
478 Images were acquired using a Zeiss LSM 980 Airyscan 2 microscope in Airyscan
479 super-resolution mode, with the default settings applied for Airyscan image
480 processing. A Plan-Apochromat 10x/0.45 or Plan-Apochromat 20x/0.8 objective was
481 employed for image acquisition (University of Leicester Advanced Imaging Facility).
482 Post-processing was performed using a custom FIJI (Schindelin *et al.*, 2012) macro
483 for orienting the embryos along anatomical axes (Embryo Processing IF Script).
484
485 **Single-cell dissociation**
486 Embryos were transferred into an ice-cold 15 mL Dounce homogeniser in PBS
487 containing Protector RNase Inhibitor, and all subsequent steps were performed at 4
488 °C to preserve RNA integrity. After three gentle washes with cold Dulbecco's PBS
489 (DPBS), the supernatant was removed and replaced with PBS supplemented with
490 0.04% BSA (PBS/BSA). Embryos were then mechanically disrupted by 10–15 strokes
491 with the tight-fitting pestle, and the homogenate was collected into a fresh tube. To
492 maximise cell recovery, the homogeniser was rinsed with additional PBS/BSA, and
493 the combined suspension was centrifuged at 3,000 × g for 3 minutes. The supernatant
494 was discarded, and the pellet was resuspended in PBS/BSA.
495 To remove large debris, the resuspended cells were centrifuged at 40 × g for 3
496 minutes, after which the supernatant—containing single cells—was transferred to a
497 new tube and spun at 1,000 × g for 3 minutes. The resulting pellet was gently triturated
498 in PBS/BSA by passing the suspension through a 22-gauge needle with 20 strokes to
499 dissociate any remaining aggregates, then filtered through a 100 µm nylon mesh. A
500 final spin at 1,000 × g for 3 minutes pelleted the cleaned single-cell suspension, which
501 was resuspended in PBS/BSA and kept on ice prior to fluorescence-activated cell
502 sorting (FACS). Parallel control samples—unstained; stained with only primary or only
503 secondary antibodies; and combinations thereof with DRAQ5 nuclear stain—were
504 prepared and processed identically for gating and compensation during FACS
505 analysis.
506

507 **FACS**

508 Cells were sorted on a Beckman Coulter MoFlo Astrios cell sorter (Nottingham)
509 equipped with a 100 µm nozzle, operating in “Purify” precision mode with a 1–2 drop
510 envelope to maximise purity of collected fractions. Single-cell suspensions were
511 maintained at 4°C throughout sorting by housing the entire flow chamber in a water-
512 cooled environment, thereby minimising heat-induced stress and preserving cell
513 integrity. Samples were deposited into a two-way tube holder pre-chilled on ice.

514 Gating strategies were defined using unstained and single-stained controls to
515 eliminate autofluorescent events. We applied broad gates to capture both strongly and
516 weakly fluorescent populations, acknowledging the continuum of marker expression.
517 $SoxN^+$ and $Elav^+$ cells—representing early neurogenic and post-mitotic neuronal
518 cohorts, respectively—were collected together. This inclusive approach ensured
519 recovery of the full spectrum of developing neural cells.

520

521 **Reverse cross-linking**

522 After FACS, the cells were subjected to a reverse cross-linking step to remove the
523 DSP fixative and prepare them for subsequent library preparation. The sorted cells
524 were first centrifuged at 4°C at 1,000 x g for 3 minutes, and the supernatant was
525 discarded. The cell pellet was then resuspended in PBS/BSA solution and incubated
526 with 50 mM dithiothreitol (DTT, Sigma-Aldrich) at 37°C for 30 minutes to break the
527 cross-links formed by DSP. Following incubation, the cells were centrifuged twice at
528 4°C at 1,000 x g for 3 minutes to thoroughly remove any residual DTT.

529

530 **10X Genomics Library Preparation**

531 The library preparation was conducted using the 10X Genomics Chromium Next GEM
532 Single Cell 3' Reagent Kit v3.1 (10X Genomics). Prior to the preparation, cell
533 concentration was assessed with a Luna FX7 Cell Counter, and cells were adjusted
534 to a concentration of approximately 500-1500 cells/µl. Approximately 8000 cells per
535 sample were used to generate single-cell gel beads in emulsion (GEMs), targeting
536 approximately 5000 single-cell GEMs per sample. GEM emulsions were created with
537 the 10X Chromium Controller, followed by complementary DNA (cDNA) synthesis and
538 library preparation according to the manufacturer's protocol. cDNA amplification was
539 performed for 12 cycles, and library amplification during the PCR indexing stage was
540 similarly carried out for 12 cycles using the Dual Index Kit TT Set A (10X Genomics).

541 Quantification of cDNA was performed using Qubit dsDNA HS assays (Invitrogen) and
542 D5000 HS ScreenTape (Agilent) on an Agilent Technologies TapeStation 4200, while
543 library quantification was conducted with Qubit dsDNA HS assays and D1000
544 ScreenTape on the same platform. Libraries were prepared following the
545 manufacturer's guidelines and were subsequently sequenced externally by Novogene
546 on the Illumina NovaSeq X Plus platform, utilising 150 bp paired-end reads.
547

548 **HCR Validation**

549 Custom probe sets targeting mRNAs of key monoaminergic pathway enzymes,
550 receptors, and TFs were designed from the longest isoform FlyBase annotations and
551 synthesised by Molecular Instruments. Briefly, embryos were first equilibrated in
552 hybridisation buffer (v3.1, Molecular Instruments) at 37°C for 30 min to block non-
553 specific sites, then incubated overnight (12–16 h) at 37°C with 4 pmol of each probe
554 set in fresh hybridisation buffer, following the manufacturer guidelines. Following this,
555 unbound probes washed, and fluorophore-conjugated HCR hairpins (Molecular
556 Instruments) were snap-cooled and applied to embryos in amplification buffer, then
557 incubated for 12–16 h at room temperature in the dark. Post-amplification, embryos
558 were washed to remove excess hairpins.

559 Finally, embryos were counterstained with DAPI (1:1000, Sigma-Aldrich) during
560 the last wash, mounted in antifade medium (Vectashield; Vector Laboratories), and
561 imaged by confocal microscopy and processed using a custom macro script in FIJI
562 (Embryo Processing HCR Script).
563

564 **Targeted Metabolomics**

565 Embryos from seven consecutive developmental windows were rinsed thoroughly in
566 distilled water to remove yeast, excess liquid discarded, weighed, and flash-frozen in
567 liquid nitrogen. Samples were shipped on dry ice to the EMBL Metabolomics Core
568 Facility (Heidelberg, Germany), where Bernhard Drotleff performed all downstream
569 processing.

570 Each frozen sample (75 mg/mL) was extracted on dry ice by adding 80%
571 acetonitrile (with internal standards and 1% formic acid), then homogenised using 1
572 mm zirconia beads in a bead-beater (FastPrep-24) at 6.0 m/s (5 × 30 s, 5 min rest).
573 After incubation at –20 °C for 20 min, lysates were vortexed and centrifuged (15 000

574 × g, 10 min, 4 °C). Supernatants were transferred to glass vials and analysed within 2
575 h.
576 LC–MS/MS was carried out on an Agilent Infinity II BioLC coupled to a Sciex
577 QTRAP 6500+ (positive ESI). Chromatography used an Atlantis Premier BEH Z-HILIC
578 column (2.1 × 100 mm, 1.7 µm) at 40 °C, with mobile phases A (90:10 H_2O:ACN) and
579 B (98:2 ACN:H_2O), both buffered with 25 mM ammonium formate (pH 3.0). The 13
580 min gradient (0–1 min 100% B; 1–8 min to 60% B; 8–10 min 60% B; 10–10.5 min to
581 100% B; 10.5–13 min 100% B) ran at 0.3 mL/min, with 5 µL injections at 4 °C. Ion
582 source parameters were: curtain gas 40 psi, nebulizer gas 40 psi, heater gas 40 psi,
583 ion spray voltage 5 kV, source temperature 400 °C, medium collision gas. Data were
584 acquired in scheduled MRM mode (90 s windows, 600 ms cycle). Samples were
585 analysed in randomised order, with pooled QCs for system equilibration and every fifth
586 sample to monitor performance; a processed blank defined background. Raw peak
587 areas were extracted and processed in SciexOS. Data analysis and visualisation was
588 done in R using custom scripts (Metabolomics R Script).
589
590 **scRNA-seq Analysis: Data alignment**
591 Raw sequencing data were processed using Cell Ranger count (v9.0.1, 10X
592 Genomics). Reads were aligned to a custom *Drosophila melanogaster* reference
593 (Ensembl release BDGP6.46.110) into which the GFP transgene sequence had been
594 incorporated. Cell Ranger generated UMI-collapsed gene–cell count matrices for each
595 library.
596
597 **scRNA-seq Analysis: Preprocessing and Quality Control**
598 Downstream quality control and preprocessing were carried out in Seurat (v5.2.0; full
599 pipeline available at GitHub page). Briefly, cells with fewer than 800 or more than 100
600 000 UMIs, fewer than 200 or more than 8 000 detected genes, or mitochondrial
601 transcript content exceeding 8–10% were excluded. After log-normalisation and
602 identification of highly variable features, JackStraw analysis was used to select
603 significant principal components for dimensionality reduction. Uniform Manifold
604 Approximation and Projection (UMAP) was then performed on these PCs. To remove
605 artifactual multiplets, DoubletFinder (v2.0.6, McGinnis, Murrow and Gartner, 2019)
606 was applied with an expected doublet rate of 3.9%, consistent with 10X Genomics
607 loading recommendations.

608 **scRNA-seq Analysis: Integration and Cluster Annotation**

609 Biological replicates from each developmental time point were integrated using
610 Harmony (v1.2.3, Korsunsky *et al.*, 2019) to correct batch effects while preserving
611 biological variation. Clusters were initially defined in the integrated UMAP space and
612 then annotated following a modified version of the Calderon *et al.* (2022) pipeline:
613 marker genes for each cluster, selected as the top differentially expressed features
614 with adjusted $P < 0.05$, were compared against curated spatial expression terms from
615 the Berkeley Drosophila Genome Project (BDGP) using Fisher's exact test to identify
616 over-represented *in situ* annotations (Tomancak *et al.*, 2002, 2007; Hammonds *et al.*,
617 2013; Calderon *et al.*, 2022). After Bonferroni correction, significant enrichment terms
618 were manually reviewed and consolidated to assign each cluster to a defined
619 neurogenic or neuronal identity. This combined data-driven and expert-curated
620 approach ensured robust annotation of cell states across *Drosophila* embryonic
621 neurogenesis.

622 To preserve the continuum of developmental variation, cells from all time points
623 were merged without additional batch-correction; standard integration algorithms
624 tended to over-correct and attenuate genuine developmental signals. The merged
625 dataset was then reclustered in Seurat, and each resulting cluster was assigned an
626 identity based on the modal annotation of its constituent cells from the individual time-
627 point analyses. This majority-vote approach ensured that clusters reflected the
628 predominant cell state across development.

629

630 **scRNA-seq Analysis: Neuronal-Specific Annotation**

631 We next focused on delineating specific neuronal lineages. Clusters corresponding to
632 the progression from neuroblasts to mature neurons were reannotated using
633 expression of subtype markers defined in Dillon *et al.* (2022) Peng *et al.* (2024). This
634 approach yielded fine-grained, cell-type annotations that aligned with, and extended,
635 the broader developmental ontology derived from BDGP enrichment annotation
636 pipeline.

637

638 **scRNA-seq Analysis: Trajectory Inference via RNA Velocity**

639 To infer cellular dynamics and developmental trajectories, Cell Ranger BAM files were
640 reprocessed with Velocyto (v0.17.17, La Manno *et al.*, 2018) to quantify spliced and

641 unspliced transcripts, producing Loom matrices. Next, the Seurat-annotated object
642 was converted to an AnnData structure using sccustomize (v3.0.1, Samuel Marsh *et*
643 *al.*, 2024), and merged with the velocity matrices preserving metadata, embeddings,
644 and clustering labels. Downstream modeling was carried out in scVelo (v0.3.3, La
645 Manno *et al.*, 2018; Bergen *et al.*, 2020) using the dynamical model: data were first
646 filtered and normalised, moments were computed on the neighborhood graph, and
647 velocity vectors were estimated for each cell. Finally, velocity-stream embeddings
648 were projected onto the UMAP embedding to visualise inferred developmental
649 progressions.
650
651 **scRNA-seq Analysis: Subclustering and Lineage Dynamic Analysis**
652 To resolve finer neuronal subtypes, we isolated cells from the maturing neuronal
653 lineage and performed a second round of clustering in Seurat. Clusters were
654 reannotated based on the expression of established subtype marker genes, and dot
655 plots were generated to verify marker specificity. We then recalculated RNA-velocity
656 on this subset in scVelo (v0.3.3, La Manno *et al.*, 2018; Bergen *et al.*, 2020), re-
657 deriving the first- and second-order moments, velocity vectors, velocity-stream
658 embedding, and latent-time projections. These velocity maps were overlaid on the
659 UMAP to visualise intra-lineage transitions. Finally, CellRank was applied to the
660 subclustered dataset—integrating connectivity, velocity, and CytoTRACE kernels—to
661 infer both initial (progenitor) and terminal (mature neuron) fates and compute fate
662 probabilities within the neuronal lineage (Reuter *et al.*, 2018; Lange *et al.*, 2022;
663 Reuter, Klein and Lange, 2022; Weiler *et al.*, 2024).
664
665 **scRNA-seq Analysis: Regulatory dynamics**
666 To uncover TFs that drive subtype specification, we performed differential expression
667 analysis restricted to TFs annotated in the AnimalTFDB for *Drosophila melanogaster*
668 (Shen *et al.*, 2023). Candidate TFs with significant up-regulation in each neuronal
669 subtype were identified and ranked. Furthermore, leveraging the latent-time ordering
670 from scVelo, we modeled the dynamic expression of all genes along developmental
671 trajectories. We then refined this analysis using CellRank's multi-kernel framework—
672 combining connectivity, velocity, and CytoTRACE information—to pinpoint TFs whose
673 expression kinetics most strongly correlate with the latent time. This layered approach

674 highlighted key regulators of neuronal differentiation for subsequent validation using
675 HCR.
676
677 **Comparative scRNAseq analysis: Dataset Acquisition and Preprocessing**
678 To explore the evolutionary conservation of these regulators, we reanalysed a
679 published *Danio rerio* developmental single-cell RNA-seq dataset spanning 10
680 developmental stages, from 10 hours post-fertilisation (hpf) to 10 days post-fertilization
681 (dpf) (Lange *et al.*, 2024). Raw sequencing data were remapped using CellRanger
682 (v9.0.1, 10x Genomics) to the zebrafish reference genome (Danio_rerio.GRCz11.114,
683 Ensembl), ensuring retention of both spliced and unspliced reads. BAM files were
684 subsequently processed with Velocyto (v0.17.17, La Manno *et al.*, 2018) to generate
685 Loom files containing spliced/unspliced transcript counts.
686
687 **Comparative scRNAseq analysis: Dataset Acquisition and Preprocessing**
688 To explore the evolutionary conservation of these regulators, we reanalysed published
689 single-cell RNA-seq datasets from *Danio rerio* and *Strongylocentrotus purpuratus*. The
690 zebrafish atlas spans 10 developmental stages from 10 hours post-fertilisation (hpf) to
691 10 days post-fertilisation (dpf) (Lange *et al.*, 2024). The sea urchin dataset was
692 generated from combining two datasets, comprising 10 time points from the 8-cell
693 stage to the 72 hpf larval stage (Foster, Oulhen and Wessel, 2020; Perillo *et al.*, 2020).
694 For zebrafish, raw 10x Genomics sequencing data were reprocessed with Cell Ranger
695 (v9.0.1; 10x Genomics) against the Ensembl *D. rerio* reference
696 (Danio_rerio.GRCz11.114), retaining both spliced and unspliced reads. Resulting
697 BAM files were converted to spliced/unspliced count matrices using Velocyto
698 (v0.17.17, La Manno *et al.*, 2018), yielding loom files for downstream analysis. For sea
699 urchin, we used the author-provided count matrices and accompanying metadata
700 without remapping.
701
702 **Comparative scRNAseq analysis: Data Integration and Annotation**
703 Rather than reclustering the full datasets, we focused on neural lineages. For
704 zebrafish, central nervous system (CNS) populations were subset using the original
705 annotations provided in the source atlas (https://zebrahub.sf.czbiohub.org/data). For
706 sea urchin, we subset to neurogenic clusters based on the authors' labels.

Cross-species re-annotation was performed with orthologous marker genes derived using eggNOG-based orthology mapping (described below), with the *Drosophila melanogaster* subclustering marker set as the anchor. For sea urchin, orthologues were called from the *S. purpuratus* proteome corresponding to the reference genome used for mapping (GCF_000002235.4; Spur_4.2). Zebrafish markers were referenced to Ensembl *D. rerio* GRCz11 (release 114). Monoaminergic neuron populations were identified by expression of the orthologous canonical biosynthetic enzymes and transporters.

Comparative scRNAseq analysis: Trajectory and Dynamic Expression Analyses

RNA velocity was estimated using scVelo (Bergen *et al.*, 2020) and lineage inference was refined with CellRank (v2) (Weiler *et al.*, 2024) by integrating connectivity and velocity information. Latent-time ordering was used to model dynamic gene expression trajectories and identify TFs with temporal activation patterns correlating with neuronal differentiation.

Comparative scRNAseq analysis: Differential Expression and Orthology Mapping

Candidate TFs enriched in each neuronal subtype were identified using the same thresholds applied to the *Drosophila* dataset (adjusted $p < 0.05$; $|\log2FC| \geq 0.25$). For cross-species comparison, we re-annotated the proteomes of zebrafish and *Drosophila* with eggNOG (v5.0, Huerta-Cepas *et al.*, 2019), assigning genes to its hierarchical orthogroup framework. We then conducted all comparative analyses at the Bilateria-level orthogroups, which consolidate one-to-many and many-to-one relationships, enabling robust mapping of putative orthologs and fair TF comparisons across species.

Comparative scRNAseq analysis: Comparative and Class-specific Analyses

Shared and species-specific regulators were identified by comparing differentially expressed TF orthogroups across *Drosophila* and zebrafish monoaminergic clusters. To contextualise these findings, the orthogroup-level analysis was extended to other neurotransmitter lineages (acetylcholine, GABA, glutamate).

740 **Data availability**

741 All data supporting this study are available on Zenodo. Processed FACS data are
742 deposited at https://doi.org/10.5281/zenodo.17449471, targeted metabolomics data at
743 https://doi.org/10.5281/zenodo.17449991, and processed single-cell RNA-seq data at
744 https://doi.org/10.5281/zenodo.17441737. All datasets are released under the MIT
745 License. Analysis pipelines and scripts are available at
746 https://github.com/cliftonlewis/2025_Drosophila_scRNAseq_EmbryoNeurogenesis_
747 Monoamine.
748

749 **Author Contributions**

750 R.F. conceived the project. C.L. performed the majority of sample preparation for
751 scRNA-seq, HCR, and targeted metabolomics, and carried out the bioinformatics
752 analyses. M.G. provided guidance on the bioinformatics analyses. A.W. assisted with
753 optimization of HCR protocols. N.C. and D.O. contributed to FACS sorting. S.R.
754 supported the initial project setup. R.P.Z. provided the initial protocols for targeted
755 scRNA-seq in *Drosophila* embryos. J.S. contributed to project development. E.R. and
756 C.P.K. supervised and supported the project. R.F. was the primary supervisor. C.L.
757 and R.F. wrote and edited the manuscript.
758

759 **Acknowledgements**

760 We gratefully acknowledge the support of the Royal Society through a University
761 Research Fellowship (UF160226 and URF/R/221011) and a Research Grant
762 (RGF\R1\181012) awarded to R.F. C.L. is supported by a BBSRC-MIBTP PhD
763 Studentship (Grant number MIBTP2020: BB/T00746X/1). The authors wish to thank
764 the technical and scientific staff of several core facilities for their invaluable support.
765 We are especially grateful for the assistance received from the University of Leicester
766 Advanced Imaging Facility (RRID: SCR_020967; BBSRC grant: BB/S019510/1) and
767 specifically thank Dr. Kees Straatman for his expert microscopy advice. This research
768 used the ALICE High Performance Computing Facility at the University of Leicester.
769 We thank the Flow Cytometry Facility, particularly Dr. David Onion and Nicola Croxall,
770 for their support with the Beckman Coulter MoFlo Astrios Flow Cytometer. We also
771 thank the DEEP-SEQ Genomics Facility, specifically Dr. Christopher Moore and Dr.

Nadine Holmes, for their expert assistance with single-cell genomics, including 10X Genomics support. Additionally, we are deeply appreciative of Dr. Bernhard Drotleff from the EMBL Metabolomics Facility for running the targeted metabolomics experiments. We would also like to thank Dr. Diego Calderon (University of California San Francisco) for help with adapting the cell type annotation pipeline. Finally, we would like to thank the Feuda Lab for their thoughtful proofreading and constructive feedback on the manuscript.

References

Arendt, D. (2005) “Genes and homology in nervous system evolution: Comparing gene functions, expression patterns, and cell type molecular fingerprints,” *Theory in Biosciences*, 124(2), pp. 185–197. Available at: https://doi.org/10.1016/j.thbio.2005.08.002.

Arendt, D. *et al.* (2019) “Evolution of neuronal types and families,” *Current Opinion in Neurobiology*, 56, pp. 144–152. Available at: https://doi.org/10.1016/j.conb.2019.01.022.

Babski, H., Codianni, M. and Bhandawat, V. (2024) “Octopaminergic descending neurons in *Drosophila*: Connectivity, tonic activity and relation to locomotion,” *Heliyon*, 10(9), p. e29952. Available at: https://doi.org/10.1016/j.heliyon.2024.e29952.

Bergen, V. *et al.* (2020) “Generalizing RNA velocity to transient cell states through dynamical modeling,” *Nature Biotechnology*, 38(12), pp. 1408–1414. Available at: https://doi.org/10.1038/s41587-020-0591-3.

Busch, S. *et al.* (2009) “A map of octopaminergic neurons in the Drosophila brain,” *The Journal of Comparative Neurology*, 513(6), pp. 643–667. Available at: https://doi.org/10.1002/cne.21966.

Cai, J. *et al.* (2009) “The role of Lmx1a in the differentiation of human embryonic stem cells into midbrain dopamine neurons in culture and after transplantation into a Parkinson’s disease model,” *Stem Cells (Dayton, Ohio)*, 27(1), pp. 220–229. Available at: https://doi.org/10.1634/stemcells.2008-0734.

Calderon, D. *et al.* (2022) “The continuum of *Drosophila* embryonic development at single-cell resolution,” *Science*, 377(6606), p. eabn5800. Available at: https://doi.org/10.1126/science.abn5800.

Campos-Ortega, J.A. and Hartenstein, V. (1985) “Stages of Drosophila Embryogenesis,” in Campos-Ortega, J. A. and Hartenstein, V., *The Embryonic Development of Drosophila melanogaster*. Berlin, Heidelberg: Springer Berlin Heidelberg, pp. 9–84. Available at: https://doi.org/10.1007/978-3-662-02454-6_3.

Cheng, L. *et al.* (2003) “Lmx1b, Pet-1, and Nkx2.2 coordinately specify serotonergic neurotransmitter phenotype,” *The Journal of Neuroscience: The Official Journal of the Society for Neuroscience*, 23(31), pp. 9961–9967. Available at: https://doi.org/10.1523/JNEUROSCI.23-31-09961.2003.

Choi, H.M.T. *et al.* (2018) “Third-generation in situ hybridization chain reaction: multiplexed, quantitative, sensitive, versatile, robust,” *Development*, 145(12), p. dev165753. Available at: https://doi.org/10.1242/dev.165753.

Dillon, N. *et al.* (2022) “Single cell RNA-seq analysis reveals temporally-regulated and quiescence-regulated gene expression in Drosophila larval neuroblasts,” *Neural Development*, 17(1), p. 7. Available at: https://doi.org/10.1186/s13064-022-00163-7.

818 Ding, Y.-Q. *et al.* (2003) “Lmx1b is essential for the development of serotonergic
819 neurons,” *Nature Neuroscience*, 6(9), pp. 933–938. Available at:
820 https://doi.org/10.1038/nn1104.

821 Dittrich, R. *et al.* (1997) “The differentiation of the serotonergic neurons in the
822 Drosophila ventral nerve cord depends on the combined function of the zinc finger
823 proteins Eagle and Huckebein,” *Development*, 124(13), pp. 2515–2525. Available at:
824 https://doi.org/10.1242/dev.124.13.2515.

825 Doucet-Beaupré, H., Ang, S.-L. and Lévesque, M. (2015) “Cell fate determination,
826 neuronal maintenance and disease state: The emerging role of transcription factors
827 Lmx1a and Lmx1b,” *FEBS Letters*, 589(24PartA), pp. 3727–3738. Available at:
828 https://doi.org/10.1016/j.febslet.2015.10.020.

829 Flames, N. and Hobert, O. (2009) “Gene regulatory logic of dopamine neuron
830 differentiation,” *Nature*, 458(7240), pp. 885–889. Available at:
831 https://doi.org/10.1038/nature07929.

832 Flames, N. and Hobert, O. (2011) “Transcriptional Control of the Terminal Fate of
833 Monoaminergic Neurons,” *Annual Review of Neuroscience*, 34(Volume 34, 2011),
834 pp. 153–184. Available at: https://doi.org/10.1146/annurev-neuro-061010-113824.

835 Foster, S., Oulhen, N. and Wessel, G. (2020) “A single cell RNA sequencing
836 resource for early sea urchin development,” *Development*, 147(17), p. dev191528.
837 Available at: https://doi.org/10.1242/dev.191528.

838 Goulty, M. *et al.* (2023) “The monoaminergic system is a bilaterian innovation,”
839 *Nature Communications*, 14(1), p. 3284. Available at: https://doi.org/10.1038/s41467-
840 023-39030-2.

841 Goulty, M. *et al.* (2025) “Monoaminergic neurons share transcriptional identity across
842 Bilaterian animals.” bioRxiv, p. 2025.10.10.679534. Available at:
843 https://doi.org/10.1101/2025.10.10.679534.

844 Grace, A.A. (2016) “Dysregulation of the dopamine system in the pathophysiology of
845 schizophrenia and depression,” *Nature Reviews. Neuroscience*, 17(8), pp. 524–532.
846 Available at: https://doi.org/10.1038/nrn.2016.57.

847 Hammonds, A.S. *et al.* (2013) “Spatial expression of transcription factors in
848 Drosophilaembryonic organ development,” *Genome Biology*, 14(12), p. R140.
849 Available at: https://doi.org/10.1186/gb-2013-14-12-r140.

850 Hartenstein, V. *et al.* (2017) “Developmental analysis of the dopamine-containing
851 neurons of the Drosophila brain,” *The Journal of comparative neurology*, 525(2), pp.
852 363–379. Available at: https://doi.org/10.1002/cne.24069.

853 Hendricks, T.J. *et al.* (2003) “Pet-1 ETS gene plays a critical role in 5-HT neuron
854 development and is required for normal anxiety-like and aggressive behavior,”
855 *Neuron*, 37(2), pp. 233–247. Available at: https://doi.org/10.1016/s0896-
856 6273(02)01167-4.

Hobert, O. (2008) “Regulatory logic of neuronal diversity: terminal selector genes and selector motifs,” *Proceedings of the National Academy of Sciences of the United States of America*, 105(51), pp. 20067–20071. Available at: https://doi.org/10.1073/pnas.0806070105.

Huerta-Cepas, J. *et al.* (2019) “eggNOG 5.0: a hierarchical, functionally and phylogenetically annotated orthology resource based on 5090 organisms and 2502 viruses,” *Nucleic Acids Research*, 47(D1), pp. D309–D314. Available at: https://doi.org/10.1093/nar/gky1085.

Karki, S. *et al.* (2023) “Serotonin signaling regulates actomyosin contractility during morphogenesis in evolutionarily divergent lineages,” *Nature Communications*, 14(1), p. 5547. Available at: https://doi.org/10.1038/s41467-023-41178-w.

Kasture, A.S. *et al.* (2018) “Big Lessons from Tiny Flies: Drosophila melanogaster as a Model to Explore Dysfunction of Dopaminergic and Serotonergic Neurotransmitter Systems,” *International Journal of Molecular Sciences*, 19(6), p. 1788. Available at: https://doi.org/10.3390/ijms19061788.

Korsunsky, I. *et al.* (2019) “Fast, sensitive and accurate integration of single-cell data with Harmony,” *Nature Methods*, 16(12), pp. 1289–1296. Available at: https://doi.org/10.1038/s41592-019-0619-0.

Kurian, M.A. *et al.* (2011) “The monoamine neurotransmitter disorders: an expanding range of neurological syndromes,” *The Lancet. Neurology*, 10(8), pp. 721–733. Available at: https://doi.org/10.1016/S1474-4422(11)70141-7.

La Manno, G. *et al.* (2018) “RNA velocity of single cells,” *Nature*, 560(7719), pp. 494–498. Available at: https://doi.org/10.1038/s41586-018-0414-6.

Lange, M. *et al.* (2022) “CellRank for directed single-cell fate mapping,” *Nature Methods*, 19(2), pp. 159–170. Available at: https://doi.org/10.1038/s41592-021-01346-6.

Lange, M. *et al.* (2024) “A multimodal zebrafish developmental atlas reveals the state-transition dynamics of late-vertebrate pluripotent axial progenitors,” *Cell*, 187(23), pp. 6742-6759.e17. Available at: https://doi.org/10.1016/j.cell.2024.09.047.

Libersat, F. and Pflueger, H.-J. (2004) “Monoamines and the Orchestration of Behavior,” *BioScience*, 54(1), pp. 17–25. Available at: https://doi.org/10.1641/0006-3568(2004)054%255B0017:MATOOB%255D2.0.CO;2.

Lundell, M.J. and Hirsh, J. (1994) “Temporal and spatial development of serotonin and dopamine neurons in the Drosophila CNS,” *Developmental Biology*, 165(2), pp. 385–396. Available at: https://doi.org/10.1006/dbio.1994.1261.

McGinnis, C.S., Murrow, L.M. and Gartner, Z.J. (2019) “DoubletFinder: Doublet Detection in Single-Cell RNA Sequencing Data Using Artificial Nearest Neighbors,” *Cell Systems*, 8(4), pp. 329-337.e4. Available at: https://doi.org/10.1016/j.cels.2019.03.003.

Monti, J.M. (2011) “Serotonin control of sleep-wake behavior,” *Sleep Medicine Reviews*, 15(4), pp. 269–281. Available at: https://doi.org/10.1016/j.smrv.2010.11.003.

Montioli, R. and Borri Voltattorni, C. (2021) “Aromatic Amino Acid Decarboxylase Deficiency: The Added Value of Biochemistry,” *International Journal of Molecular Sciences*, 22(6), p. 3146. Available at: https://doi.org/10.3390/ijms22063146.

Parent, A. (1984) “Functional Anatomy and Evolution of Monoaminergic Systems,” *American Zoologist*, 24(3), pp. 783–790. Available at: https://doi.org/10.1093/icb/24.3.783.

Peng, D. *et al.* (2024) “Organogenetic transcriptomes of the Drosophila embryo at single cell resolution,” *Development (Cambridge, England)*, 151(2), p. dev202097. Available at: https://doi.org/10.1242/dev.202097.

Perillo, M. *et al.* (2020) “Regulation of dynamic pigment cell states at single-cell resolution,” *eLife*, 9, p. e60388. Available at: https://doi.org/10.7554/eLife.60388.

Peter, I.S. and Davidson, E.H. (2011) “Evolution of gene regulatory networks controlling body plan development,” *Cell*, 144(6), pp. 970–985. Available at: https://doi.org/10.1016/j.cell.2011.02.017.

Rapti, G. (2022) “Open Frontiers in Neural Cell Type Investigations; Lessons From Caenorhabditis elegans and Beyond, Toward a Multimodal Integration,” *Frontiers in Neuroscience*, 15. Available at: https://doi.org/10.3389/fnins.2021.787753.

Reuter, B. *et al.* (2018) “Generalized Markov State Modeling Method for Nonequilibrium Biomolecular Dynamics: Exemplified on Amyloid β Conformational Dynamics Driven by an Oscillating Electric Field,” *Journal of Chemical Theory and Computation*, 14(7), pp. 3579–3594. Available at: https://doi.org/10.1021/acs.jctc.8b00079.

Reuter, B., Klein, M. and Lange, M. (2022) “pyGPCCA - python GPCCA: Generalized Perron Cluster Cluster Analysis package to coarse-grain reversible and non-reversible Markov state models.” Zenodo. Available at: https://doi.org/10.5281/zenodo.6914001.

Sachkova, M., Modepalli, V. and Kittelmann, M. (2025) “The Deep Evolutionary Roots of the Nervous System,” *Annual Review of Neuroscience*, 48(Volume 48, 2025), pp. 311–329. Available at: https://doi.org/10.1146/annurev-neuro-112723-040945.

Samuel Marsh *et al.* (2024) “samuel-marsh/scCustomize: Version 3.0.1.” Zenodo. Available at: https://doi.org/10.5281/ZENODO.5706430.

Sarov, M. *et al.* (2016) “A genome-wide resource for the analysis of protein localisation in Drosophila,” *eLife*. Edited by H.J. Bellen, 5, p. e12068. Available at: https://doi.org/10.7554/eLife.12068.

Schindelin, J. *et al.* (2012) “Fiji: an open-source platform for biological-image analysis,” *Nature Methods*, 9(7), pp. 676–682. Available at: https://doi.org/10.1038/nmeth.2019.

Shen, W.-K. *et al.* (2023) “AnimalTFDB 4.0: a comprehensive animal transcription factor database updated with variation and expression annotations,” *Nucleic Acids Research*, 51(D1), pp. D39–D45. Available at: https://doi.org/10.1093/nar/gkac907.

Tomancak, P. *et al.* (2002) “Systematic determination of patterns of gene expression during Drosophila embryogenesis,” *Genome Biology*, 3(12), p. research0088.1. Available at: https://doi.org/10.1186/gb-2002-3-12-research0088.

Tomancak, P. *et al.* (2007) “Global analysis of patterns of gene expression during Drosophilaembryogenesis,” *Genome Biology*, 8(7), p. R145. Available at: https://doi.org/10.1186/gb-2007-8-7-r145.

Volkow, N.D. *et al.* (2011) “Motivation deficit in ADHD is associated with dysfunction of the dopamine reward pathway,” *Molecular Psychiatry*, 16(11), pp. 1147–1154. Available at: https://doi.org/10.1038/mp.2010.97.

Waddell, S. (2013) “Reinforcement signalling in Drosophila; dopamine does it all after all,” *Current Opinion in Neurobiology*, 23(3), pp. 324–329. Available at: https://doi.org/10.1016/j.conb.2013.01.005.

Weiler, P. *et al.* (2024) “CellRank 2: unified fate mapping in multiview single-cell data,” *Nature Methods*, 21(7), pp. 1196–1205. Available at: https://doi.org/10.1038/s41592-024-02303-9.

Wijnen, H. *et al.* (2006) “Control of Daily Transcript Oscillations in Drosophila by Light and the Circadian Clock,” *PLOS Genetics*, 2(3), p. e39. Available at: https://doi.org/10.1371/journal.pgen.0020039.

Yamamoto, K. and Vernier, P. (2011) “The Evolution of Dopamine Systems in Chordates,” *Frontiers in Neuroanatomy*, 5. Available at: https://doi.org/10.3389/fnana.2011.00021.

Zheng, Q. *et al.* (2025) “Bidirectional histone monoaminylation dynamics regulate neural rhythmicity,” *Nature*, 637(8047), pp. 974–982. Available at: https://doi.org/10.1038/s41586-024-08371-3.

Figures

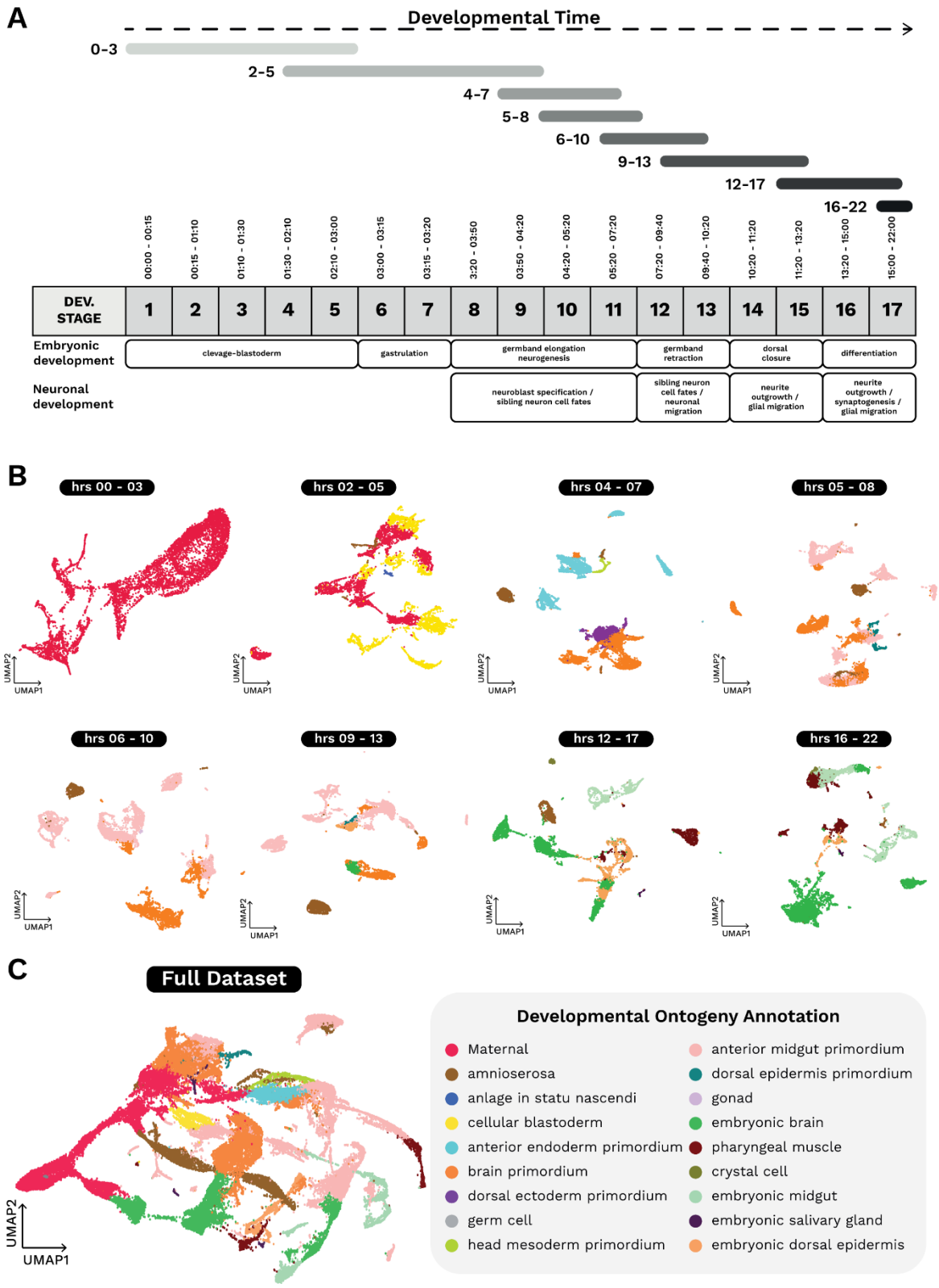
A
Developmental Time
0-3
2-5
4-7
5-8
6-10
9-13
12-17
16-22
00:00 - 00:15
00:15 - 01:10
01:10 - 01:30
01:30 - 02:10
02:10 - 03:00
03:00 - 03:15
03:15 - 03:20
3:20 - 03:50
03:50 - 04:20
04:20 - 05:20
05:20 - 07:20
07:20 - 09:40
09:40 - 10:20
10:20 - 11:20
11:20 - 13:20
13:20 - 15:00
15:00 - 22:00
DEV. STAGE
1 2 3 4 5 6 7 8 9 10 11 12 13 14 15 16 17
Embryonic development
clevage-blastoderm
gastrulation
germband elongation neurogenesis
germband retraction
dorsal closure
differentiation
Neuronal development
neuroblast specification / sibling neuron cell fates
sibling neuron cell fates / neuronal migration
neurite outgrowth / glial migration
neurite outgrowth / synaptogenesis / glial migration
B
hrs 00 - 03
hrs 02 - 05
hrs 04 - 07
hrs 05 - 08
hrs 06 - 10
hrs 09 - 13
hrs 12 - 17
hrs 16 - 22
UMAP1
UMAP2
C
Full Dataset
Developmental Ontogeny Annotation
Maternal
amnioserosa
anlage in statu nascendi
cellular blastoderm
anterior endoderm primordium
brain primordium
dorsal ectoderm primordium
germ cell
head mesoderm primordium
anterior midgut primordium
dorsal epidermis primordium
gonad
embryonic brain
pharyngeal muscle
crystal cell
embryonic midgut
embryonic salivary gland
embryonic dorsal epidermis

968 **Figure 1. Time-resolved sampling strategy and developmental ontogeny**
969 **annotation of targeted scRNA-seq across *Drosophila* embryogenesis.**

970 **A.** Timeline of eight partially overlapping collection windows, spanning
971 embryogenesis, from 0–22 hrs after egg laying (AEL) aligned to canonical embryonic
972 stages (Bownes stages 1–17, (Campos-Ortega and Hartenstein, 1985)) and key
973 morphogenetic landmarks (cleavage/blastoderm, gastrulation, germband elongation,
974 germband retraction, dorsal closure, and differentiation). Major neurogenic milestones
975 are indicated below the timeline, including neuroblast specification, diversification of
976 sibling neuron fates, neuronal migration, neurite outgrowth, glial migration, and
977 synaptogenesis. **B.** UMAPs for each time window showing single-cell transcriptomes
978 coloured by developmental ontology. **C.** UMAP of the combined dataset with cells
979 coloured by developmental ontology derived from *in situ*–guided annotation.
980 Representative labels include maternal, cellular blastoderm, amnioserosa, dorsal
981 ectoderm primordium, brain primordium, embryonic brain, and embryonic midgut.
982

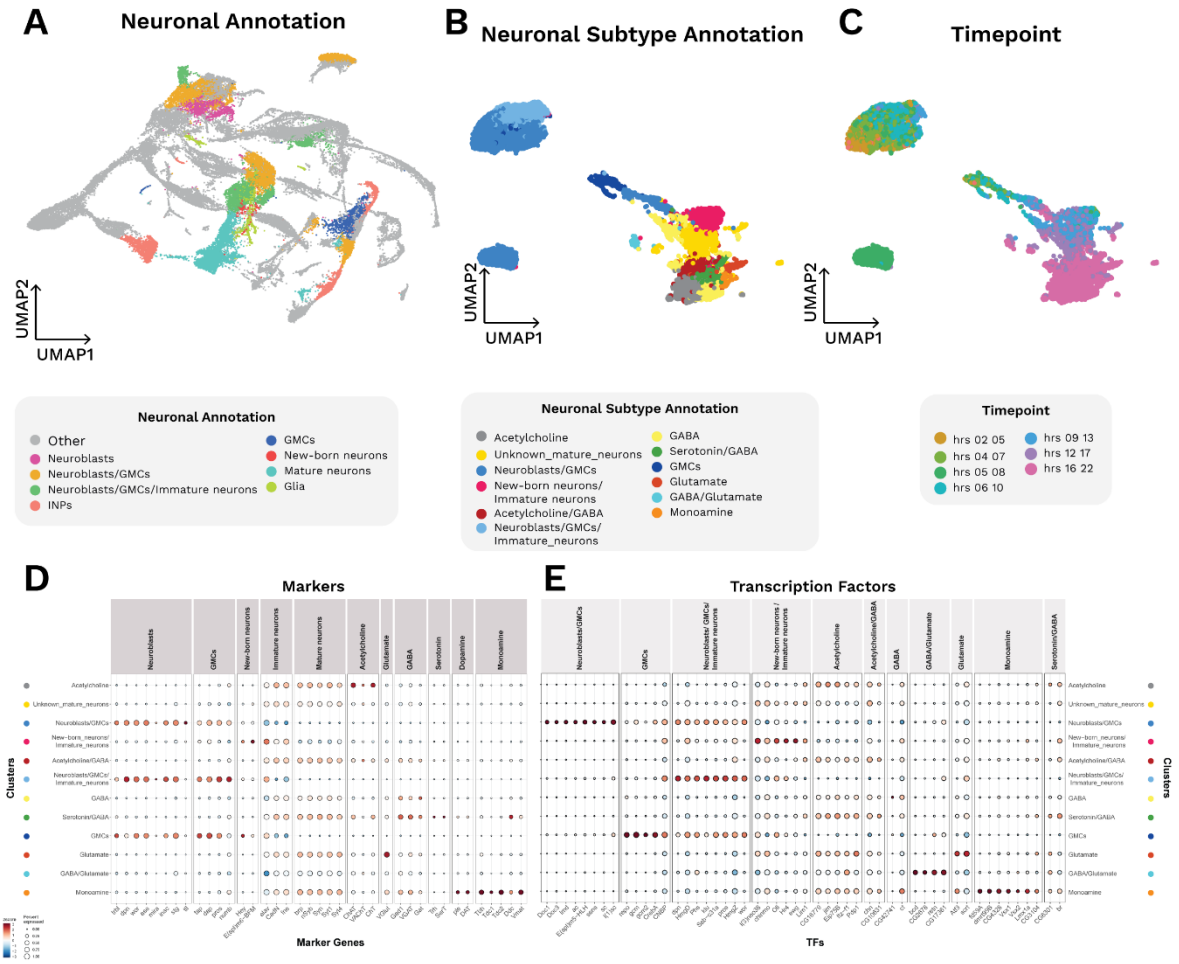

Figure 2. Time-resolved single-cell landscape of embryonic neurogenesis in Drosophila

A. Neuronal annotation. UMAP of the full embryonic dataset with neural lineages highlighted and non-neuronal cells in grey. Colours denote major neural states: neuroblasts, neuroblasts/GMCs, neuroblasts/GMCs/immature neurons, intermediate neural progenitors (INPs), GMCs, new-born/immature neurons, mature neurons, and glia. **B. Neuronal subtype annotation.** Subclustered neurogenic atlas reannotated to subtypes including transmitter-class/subtype as well as neuronal developmental intermediates. Classes include acetylcholine, GABA, glutamate, monoamine, mixed identities (e.g., acetylcholine/GABA; GABA/glutamate), unknown mature neurons, and progenitor states (neuroblasts/GMCs; neuroblasts/GMCs/immature neurons; GMCs; new-born/immature neurons). **C. Timepoint.** Subclustered dataset coloured by collection window, showing temporal separation across the UMAP. **D. Markers.** Dot plot of selected marker genes across the neuronal states/subtypes in the subclustered dataset. Dot size indicates the fraction of cells expressing the gene; colour reflects average expression. **E. Differential transcription factors.** Dot plot of differential TFs across neuronal states/subtypes, highlighting regulators associated with progenitors, early differentiation, transmitter specification, and mature neurons.

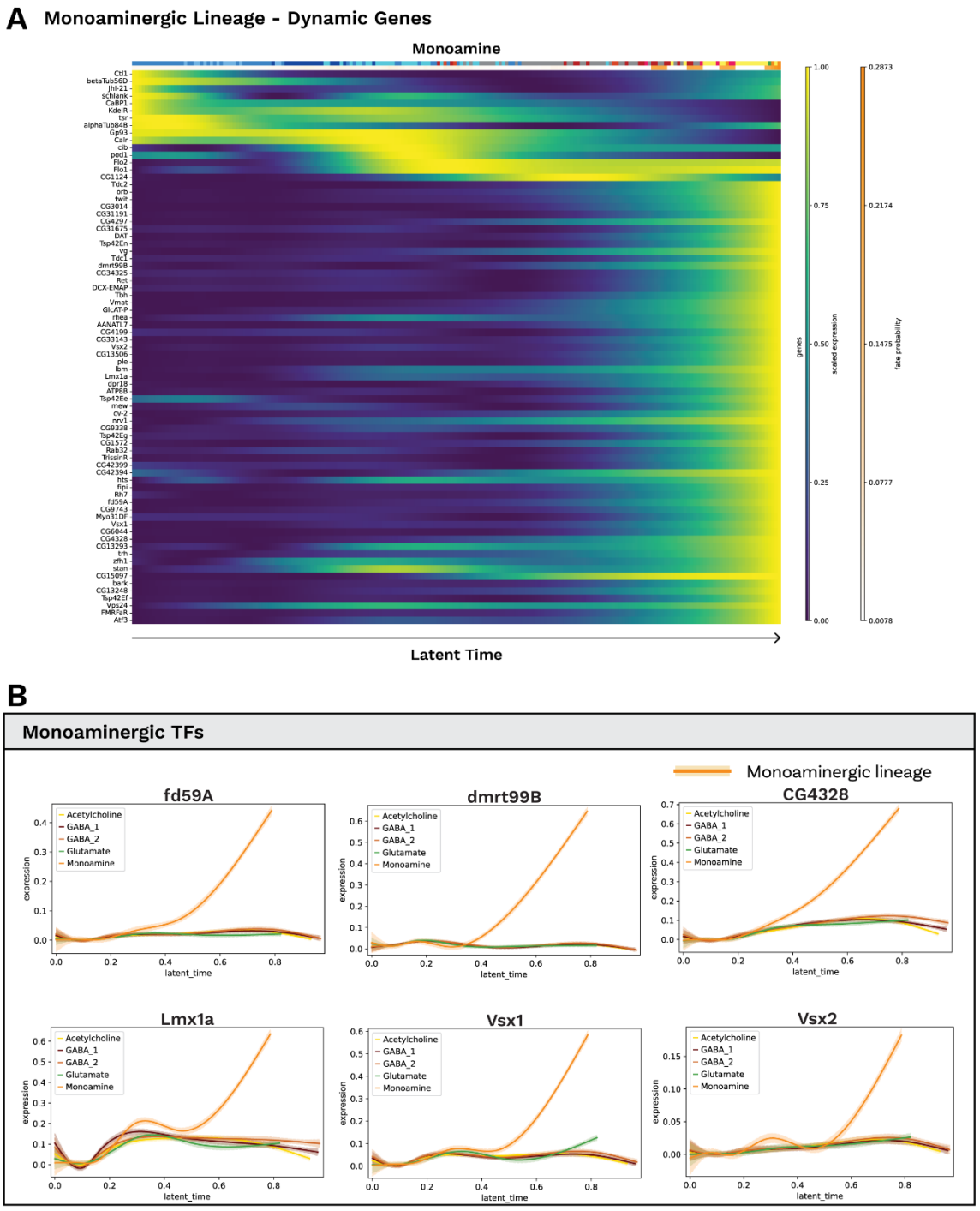

Figure 3. Monoaminergic lineage—dynamic gene programs and candidate transcription factors gene trends

A. Dynamic genes along latent time. Heatmap of CellRank-identified dynamical genes within the monoaminergic lineage. Cells are ordered by latent time (left→right; arrow) and expression is z-scaled per gene (yellow = higher expression). Many neurotransmitter-pathway genes and regulators turn on progressively toward late latent time as well as many of the candidate differentially expressed TFs identified

previously. **B. Monoaminergic transcription factors.** Smoothed expression trajectories across latent time for selected TFs (*fd59A*, *dmrt99B*, *CG4328*, *Lmx1a*, *Vsx1*, *Vsx2*). The monoaminergic lineage is highlighted in orange; other neuronal lineages (acetylcholine, GABA_1/2, glutamate) are shown for comparison. Curves show lineage-wise mean trends (y-axis, scaled expression) across latent time (x-axis), illustrating the preferential late-stage upregulation of these TFs in the monoaminergic lineage specifically.

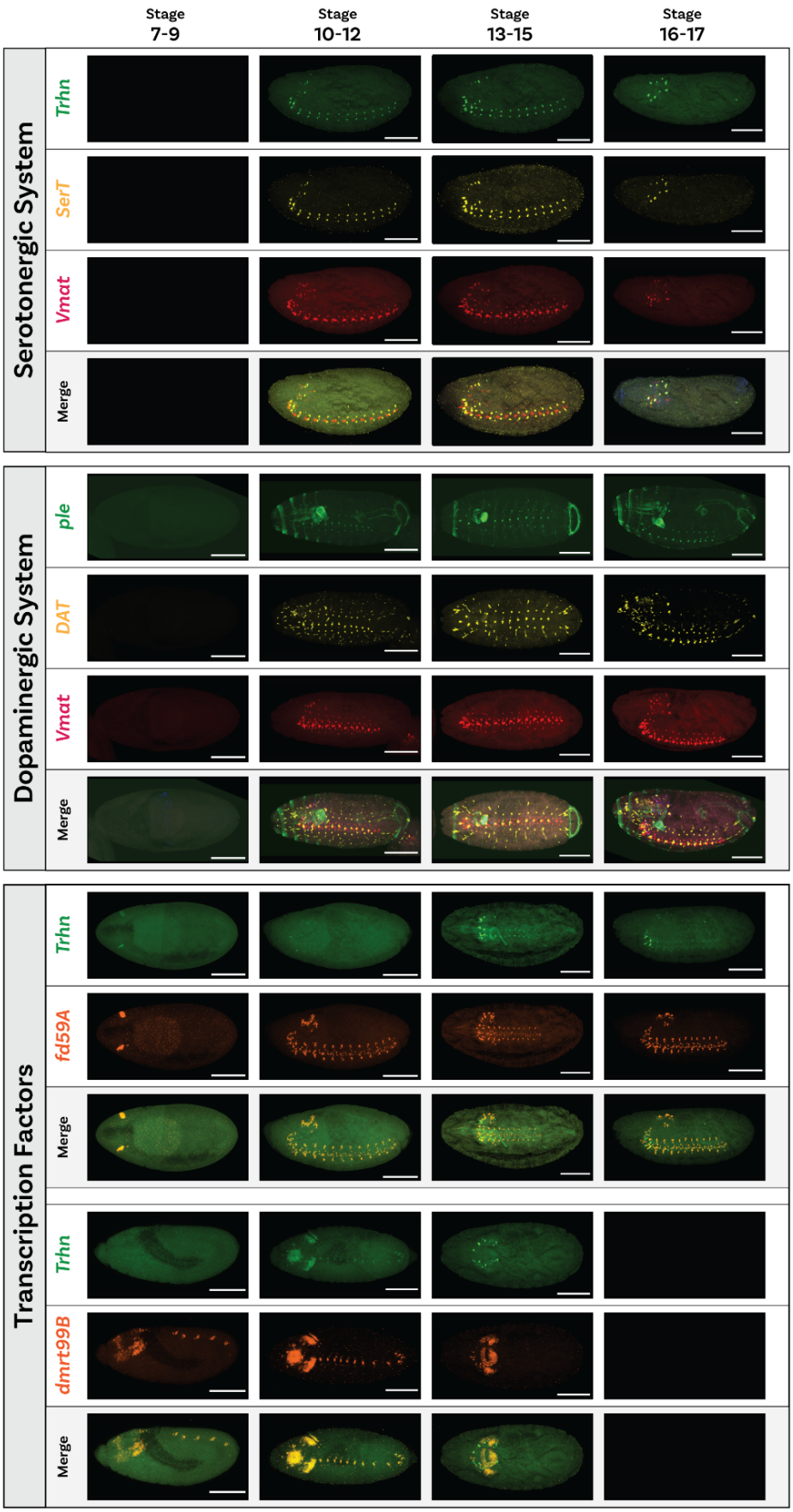
Stage 7-9
Stage 10-12
Stage 13-15
Stage 16-17
Serotonergic System
Trhn
SerT
Vmat
Merge
Dopaminergic System
ple
DAT
Vmat
Merge
Transcription Factors
Trhn
fd59A
Merge
Trhn
dmrt99B
Merge

1017

Figure 4. HCR validates the temporal onset and spatial organisation of serotonergic and dopaminergic programs in the embryo

HCR staining across four developmental windows (columns: stages 7–9, 10–12, 13–15, 16–17). Each image shows a whole-mount embryo, lateral view with anterior to the left. Scale bars 100 µm. **Serotonergic system**. HCR for *Trhn* (*tryptophan hydroxylase*, green), *SerT* (*serotonin transporter*, yellow) and *Vmat* (*vesicular monoamine transporter*, magenta), plus merges. No signal is detected at stages 7–9. From stage 10–12 onwards *Trhn*, *SerT* and *Vmat* appear in segmentally repeated CNS domains; marking serotonergic neurons as they mature. **Dopaminergic system**. HCR for *ple* (*Tyrosine hydroxylase*, green), *DAT* (*dopamine transporter*, yellow) and *Vmat* (magenta), plus merges. *ple* is first detected by stage 10–12, with *DAT* and *Vmat* also appearing by stage 10-12. *ple*/*DAT* signals co-localise with *Vmat* in the CNS. **Transcription factors**. HCR for *fd59A* or *dmrt99B* (orange) together with *Trhn* (green), plus merges. TF expression is evident in the CNS earlier (stages 7-9) and broadens by stages 10-12, preceding with enzyme onset, consistent with a putative upstream regulatory role in monoaminergic fate.

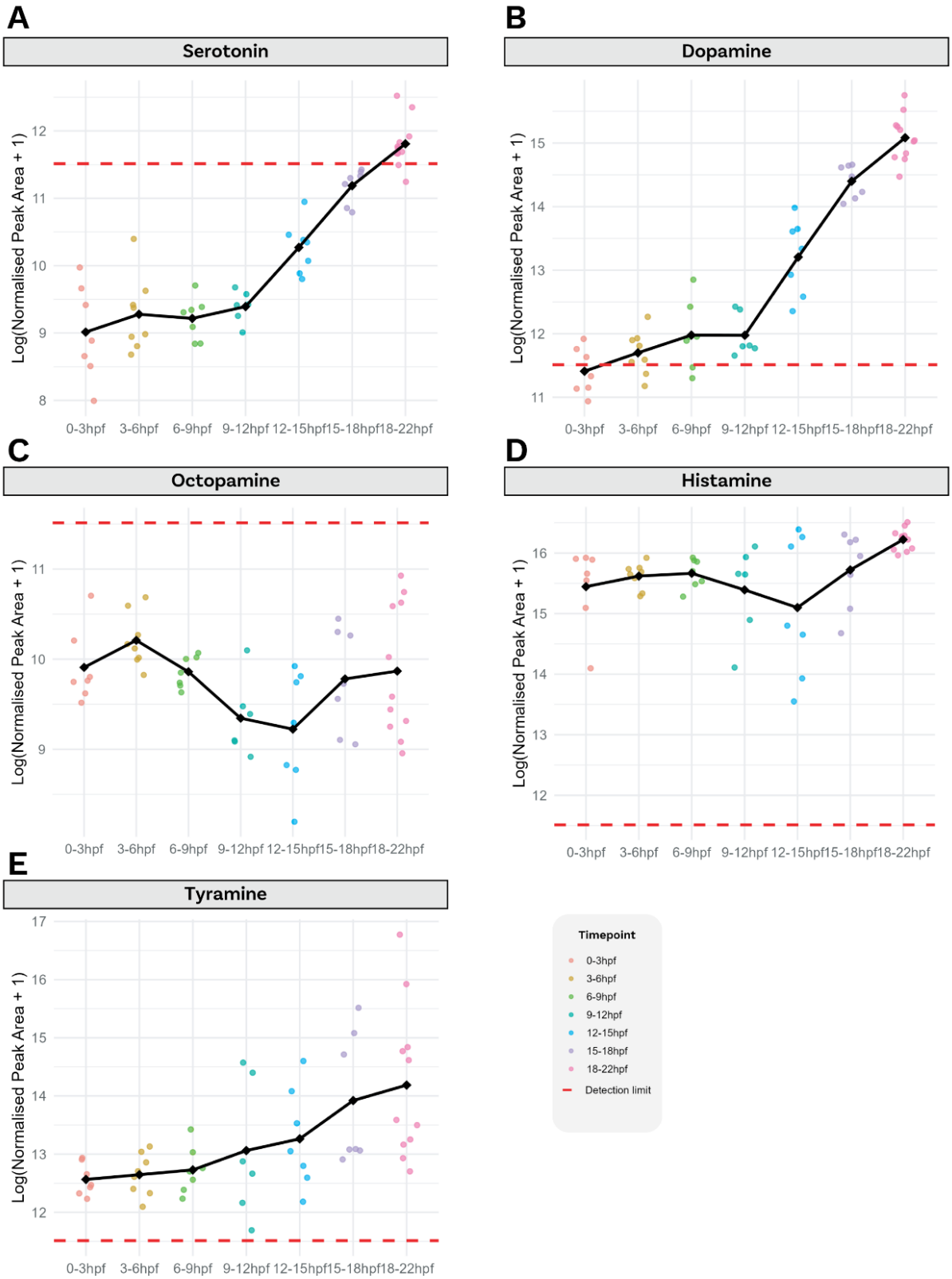
A
Serotonin
Log(Normalised Peak Area + 1)
0-3hpf
3-6hpf
6-9hpf
9-12hpf
12-15hpf
15-18hpf
18-22hpf
B
Dopamine
C
Octopamine
D
Histamine
E
Tyramine
Timepoint
0-3hpf
3-6hpf
6-9hpf
9-12hpf
12-15hpf
15-18hpf
18-22hpf
Detection limit

Figure 5. Targeted metabolomics across embryonic time reveals distinct onset of monoamine production

A–E. Concentrations of five monoamines measured by targeted LC–MS/MS across seven developmental windows (0–3, 3–6, 6–9, 9–12, 12–15, 15–18, 18–22 h AEL). Each dot is one biological replicate (≥6 per time point); colour encodes the time window. The black line connects the mean of replicates at each time. The y-axis shows $\log_{10}$(normalised peak area + 1). The red dashed line marks the empirical detection threshold for each analyte. **A. Serotonin** and **B. Dopamine:** low/near-baseline early, followed by a sharp rise beginning ~12–15 h, consistent with the transcriptional induction of biosynthetic enzymes. **C. Octopamine:** largely under the detection threshold. **D. Histamine** and **E. Tyramine**: detectable throughout development with gradual increases. Together, these profiles indicate that the functional availability of serotonin and dopamine lags their transcriptional commitment, whereas histamine and tyramine are present earlier and more continuously.

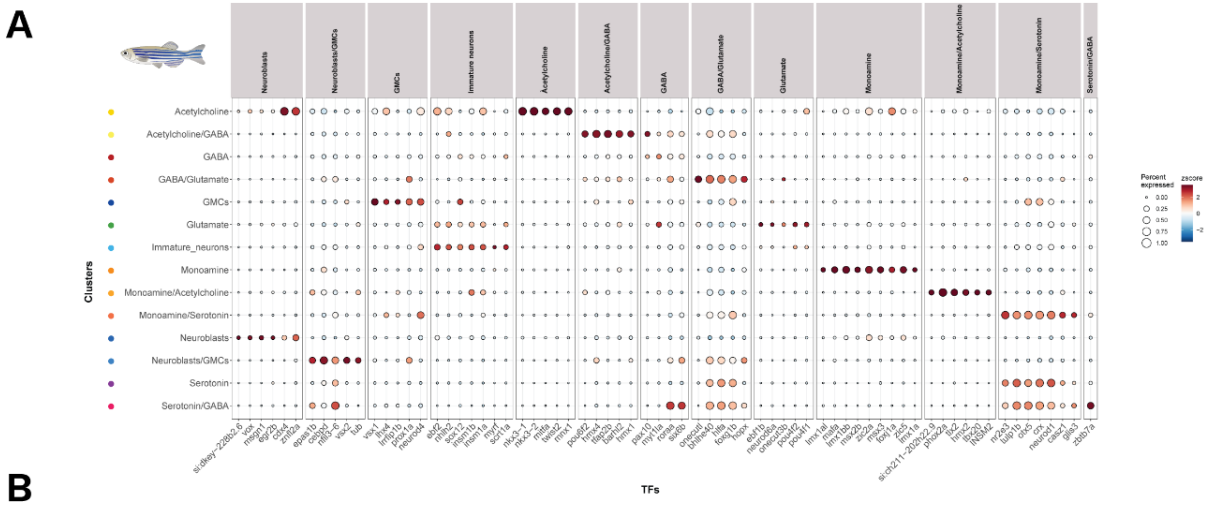

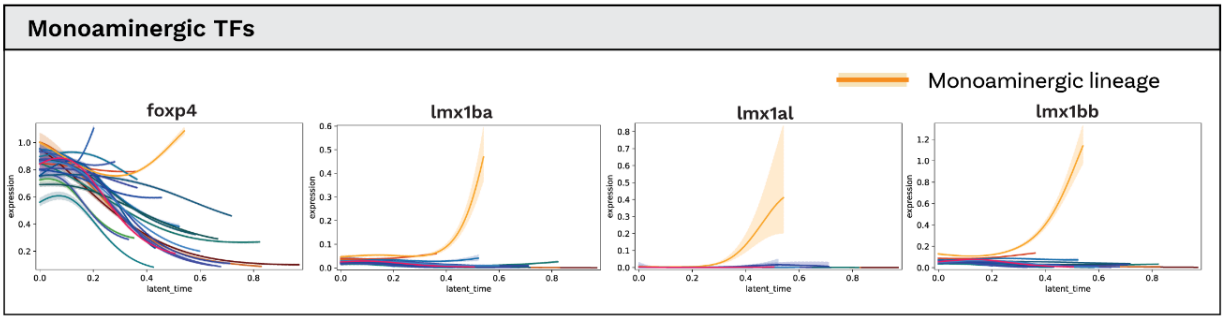

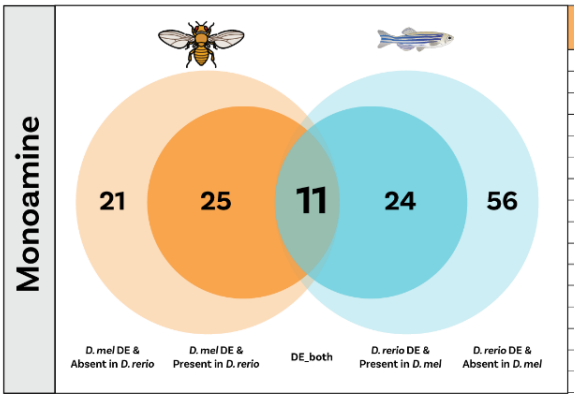

Conserved TF Orthogroups

D. melanogaster	*D. rerio*
cic	*cica*
Nfl	*nfia; nfixb*
cbt	*klf11b; klf11a*
CG4328; Lmx1a	*lmx1bb; lmx1al; lmx1ba*
FoxP	*foxp4*
trh	*NPAS3*
Eip78C	*nr1d1*
net	*atoh8*
tj	*mafa; mafb*
Pdp1	*hlfa*
luna	*klf6a*

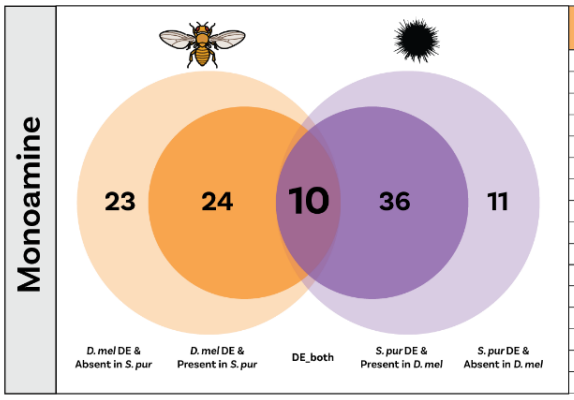

Conserved TF Orthogroups

D. melanogaster	*S. purpuratus*
Vsx1;Vsx2	*LOC575706*
zfh1	*LOC594820*
CG4328;Lmx1a	*LOC585635*
Hr3	*LOC578618*
NFAT	*LOC590859*
Tusp	*LOC591879*
fd59A	*LOC751845*
Hr38	*LOC581160*
CG3104	*LOC592680*
Eip75B	*LOC592902*

Figure 6. Cross-species conservation of monoaminergic TF programs

A. Differentially expressed TFs in *D. rerio* neurogenic subtypes. Dot plot of differentially expressed TFs across zebrafish neurogenic subtypes. Columns are grouped by transmitter/state classes (Acetylcholine, Glutamate, GABA, Serotonin, Dopamine, Monoamine; plus, developmental states such as Neuroblasts, GMCs, Immature/Mature neurons). Dot size shows the fraction of cells in the subtype expressing the TF; colour shows the z-scored average expression. **B. Monoaminergic TF dynamics.** Smoothed latent-time expression trajectories for TFs associated with monoaminergic fate (examples shown: *foxp4*, *lmx1ba*, *lmx1a1*, *lmx1a*). Curves are plotted for the major neuronal lineages; the monoaminergic lineage is highlighted in orange with a light-orange confidence band, illustrating late-latent-time up-regulation of these TFs along the monoaminergic trajectory. **C. Orthogroup-level conservation analysis.** Venn diagram summarising Bilateria eggNOG orthogroups containing TFs that are differentially expressed in monoaminergic clusters in *D. melanogaster* and *D. rerio* (criteria as in Methods: adjusted $p < 0.05$; $|\log2FC| \geq 0.25$). Left/right circles denote species-specific DE orthogroups; the intersection denotes orthogroups DE in both species. The table lists representative conserved TF orthogroups with the corresponding gene names in each species. Together, these panels show that a core set of TF orthogroups is shared across insects and vertebrates while each lineage also exhibits species-specific components of the monoaminergic program.